

---

# Decomposition of Diffuse Reflectance Images – Features for Monitoring Structure in Turbid Media

Jacob Lercke Skytte<sup>a</sup>, Otto H. A. Nielsen<sup>a,b</sup>, Ulf Andersen<sup>c</sup>, Jens Michael Carstensen<sup>a</sup>, Anders L. Dahl<sup>a</sup>, Rasmus Larsen<sup>a</sup>, Flemming Møller<sup>d</sup>, Faisal Kamran<sup>e</sup>, Jeppe Revall Frisvad<sup>a</sup>

<sup>a</sup> DTU Compute, Department of Applied Mathematics and Computer Science, Technical University of Denmark, Matematiktorvet, Building 303B, DK-2800 Kgs. Lyngby, Denmark

<sup>b</sup> NKT Photonics A/S, Blokken 84, DK-3460 Birkerød, Denmark

<sup>c</sup> Arla Strategic Innovation Centre, Rørdrumvej 2, DK-8220 Brabrand, Denmark

<sup>d</sup> DuPont, Edwin Rahrs Vej 38, DK-8220 Brabrand, Denmark

<sup>e</sup> DTU Photonics, Technical University of Denmark, Ørsteds Plads, Building 343, DK-2800 Kgs. Lyngby, Denmark

---

## ABSTRACT

**Light scattering in turbid media can be related to the microstructure of media. Thus, light scattering can potentially be used for process control of products where the structure is a key component. However process control requires robust and sensitive input data to function properly. In this study we investigate different decomposition methods for extracting light scattering information from images of diffuse reflectance. Both well-established theoretical methods and data driven methods are considered and evaluated based on their robustness and sensitivity to changes in light scattering properties.**

## 1 Introduction

Many food processes can be seen as controlled efforts to preserve, destroy, or transform structure (Aguilera et al. 1999). According to (Bourne 2002) the textural properties of foods can be derived from their structure, and is one of the most important factors concerning consumer acceptability. Microstructure in particular affects the physical properties of a material. Concerning food products the microstructure can affect a lot of the quality parameters we associate with a product, such as nutritious properties, stability, and physical properties (Aguilera 2005). Thus, there is incentive for having improved control of the structural changes during food processing in order to ensure high and consistent quality.

In this paper we investigate the potential for process control of structural changes using a novel hyperspectral imaging modality. The method is applicable for homogenous turbid media, and incorporates elements from optics and hyperspectral imaging. Data from this modality is highly dependent on the optical properties. Typically changes in the optical properties have been characterized by looking at: changes in diffuse reflectance (Payne et al. 1993), the transport mean free path ( $mfp'$ ) derived from speckle dynamics (Weitz et al. 1993, Alexander et al. 2006), and absorption ( $\mu_a$ ) and reduced scattering ( $\mu_s'$ ) (Farrell et al. 1992, Wang et al. 1995). In terms of interpretability the extraction of  $mfp'$ ,  $\mu_a$ , and  $\mu_s'$  makes it easier to relate optical properties to chemical and structural properties of turbid media. However modelling physical parameters will often introduce model variance, which can affect the robustness of the parameter estimation.

Hyperspectral imaging is a technique that integrates conventional imaging and spectroscopy. It has become increasingly popular within the field of food science during the last two decades due to speed and also non-contact assessment (Sun 2010). Gowen et al. (2007) gives an overview of recent publications within the hyperspectral imaging field, which exclusively covers heterogeneous materials such as vegetables and fruit. As we are dealing with homogenous turbid media, we take a different approach than conventional hyperspectral imaging. Rather than capturing images of a material in full field illumination, we shine a coherent, collimated light (laser) into the material and capture an image of the spatial distribution of the diffuse reflectance. These images make up the data used in our analysis.

Instead of using entire images for the analysis, a common step is to decompose an image into a number of features. This can reduce the computational load as well as provide higher level of interpretation of the diffuse reflectance images. Well-founded theoretical models will be considered for this decomposition step. These usually operate on one-dimensional intensity profiles. Also considered, are the data-driven methods that can be seen as empirical methods. These consider more of the information in the diffuse reflectance images.

The goal of this paper is to investigate different decomposition methods and evaluate their sensitivity towards changes in the scattering properties. The goal is also to determine how robust the decomposition schemes are. In order to use the image features for process control, a reasonable signal-to-noise ratio (SNR) must be established (MacGregor et al. 1995). The turbid media considered in this paper are fat emulsions. However, we expect that the methods presented here apply to homogenous turbid media in general. In terms of structure prediction, we assume that all structural information can be related to scattering.

## 2 Material

### 2.1 Diffuse Reflectance Images

When light refracts into a turbid medium it is either scattered or absorbed when interacting with the particles in the medium. Whereas absorption is highly dependent on the chemical composition of the material, scattering is highly dependent on the size, shape, and density of the particles. Thus scattering can be correlated to the microstructural properties of a material. If light only scatters, it will eventually emerge at the surface at a point different from the point of entry. The emergent light is known as the diffuse reflectance. The spatial distribution of the diffuse reflectance will typically follow an anisotropic diffusion process, which emanates from the point where the light was incident. Light close to the point of incidence has typically scattered a few times, whereas light far away from the point of incidence has scattered multiple times.

Our aim is to extract information on the optical properties from the diffuse reflectance. The system works by shining a laser with tuneable wavelength into the sample material at an oblique incident angle ( $45^\circ$ ). High Dynamic Range (HDR) images (Mann and Picard 1994) of the resulting diffuse reflectance are captured by a CCD camera (*Grasshopper CCD Cam, Point Grey Research Inc., Richmond, Canada*) with a zoom lens (*23FM50L, Tamron Co. Ltd., Saitama, Japan*) installed in front of the CCD with a 6.5cm spacer. The HDR images are 1200 by 1600 pixels, with a physical pixel size of  $3.2\mu\text{m}$ . The light delivery system is based on a super continuum light source (*SuperK Extreme, NKT Photonics, Birkerød, Denmark*), filtered by an acousto-optic tunable filter (*SuperK Select, NKT Photonics, Birkerød, Denmark*). At the moment the system potentially covers the wavelengths 450nm to 1050nm with a spectral resolution down to 5nm. As this paper is about the decomposition of the diffuse reflectance images, we will only consider a small selection of wavelengths.

A simplified schematic of the system is shown in Fig. 1 alongside an example of the diffuse reflectance images. The system is a research platform, which can be used to design cost-efficient vision systems with geometry and wavelengths optimized for a specific process. More information on the vision system is provided by Nielsen et al. (2011).

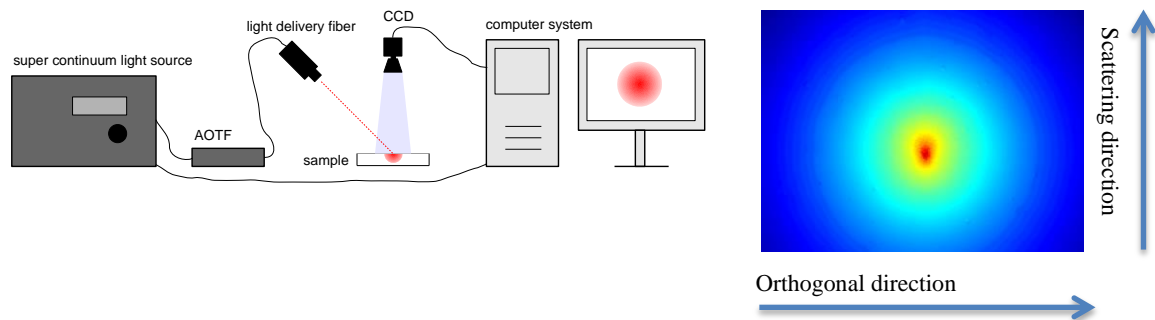


**Fig. 1** Left: Schematic of the hyperspectral vision system. Right: Example of a logarithmic transformed diffuse reflectance image. The light is shone from the bottom of the image, and the point of incidence is the area with largest pixel intensity (red colour).

### 2.2 Intralipid Data Set

The data set of this paper consists of different dilutions of Intralipid (*Intralipid 20%, Fresenius Kabi, Bad Homburg, Germany*). Intralipid is a highly stable and standardized fat emulsion and approved for direct intravenous infusion for patients who are unable to get nutrition via an oral diet. It is also often used to simulate the optical properties of turbid media, as it mainly contributes as a scattering compound in the visible regime. Turbid media are generally highly scattering materials with low absorption characteristics, i.e. the reduced scattering coefficient  $\mu_s'$  dominates over the absorption coefficient  $\mu_a$ , and incorporates many biological samples including a wide variety of food products (fruit, vegetables, dairy products, emulsions), when considering the

visible spectrum. For our experiment we made 21 graduated water dilutions of Intralipid. The dilutions were made to have linearly increasing scattering properties covering the range of milk and fermented milk products. Seven repeated measurements were made for each of the 21 dilutions, and the 21 dilutions were split into three scattering regimes of equal size, with “low”, “medium”, and “high” scattering properties. All dilutions were recorded at three different wavelengths (500, 700, and 900nm). The theoretical reduced scattering coefficients for the data set were calculated based on Lorenz-Mie theory (Frisvad et al. 2007, Michels et al. 2008), and are summarized in Table 1.

**Table 1** The theoretical reduced scattering coefficient intervals for the three selected scattering regimes at three different wavelengths. All reported intervals have the unit [ $\text{cm}^{-1}$ ]

	Low scattering regime	Medium scattering regime	High scattering regime
500nm	[7.2 ; 31.3]	[35.0 ; 63.0]	[67.5 ; 87.5]
700nm	[6.4 ; 22.2]	[24.6 ; 42.9]	[45.8 ; 59.0]
900nm	[6.0 ; 16.9]	[18.6 ; 31.3]	[33.3 ; 42.4]

### 3 Methods

It is hard to obtain information about material properties directly from the diffuse reflectance images, so the images were decomposed into compact representations (features). Two different decomposition strategies were considered. First, the theoretical models, which are commonly used for decomposing light diffusion signals into  $\mu_a$  and  $\mu_s'$ . These models are typically only based on what corresponds to intensity profiles in the images. Hereby they only utilise a fraction of the data available from our images. The second strategy therefore consisted of data-driven approaches, which utilise different parts of the images. These more empirical features are typically a mixture of the absorption and scattering properties, and can therefore be harder to interpret compared to the theoretical models. We consider different approaches to both the theoretical modelling and empirical strategies in the following. All methods are implemented using Matlab (*MathWorks, Natick, Massachusetts, U.S.A.*).

#### 3.1 Farrell Model Decomposition (FM)

General cases of light scattering and absorption in turbid media can be described analytically by the radiative transfer equation (Chandrasekhar 1960). However this expression is difficult to solve and computational inefficient for use in real time applications. For materials where scattering is dominant ( $\mu_s' \gg \mu_a$ ), the light transport can be considered a diffusion process. By assuming that diffusion is isotropic the radiative transfer equation can be simplified significantly. While this simplification cannot accurately model the diffuse reflectance near the point of incidence, it provides an efficient way of estimating  $\mu_a$  and  $\mu_s'$ .

Farrell et al. (1992) derived an analytical solution for the diffusion approximation to describe the diffuse reflectance at the surface of a semi-infinite turbid medium, when illuminated by a ray of light at normal incidence. The reduced scattering coefficient was estimated by partly following the fitting routine used in the work by Qin and Lu (2004). An inherent problem with the Farrell decomposition is that it requires absolute values of the diffuse reflectance in order to estimate the actual reduced scattering coefficient. However, for some applications it should be sufficient to look at relative estimates of the reduced scattering coefficients.

#### 3.2 Oblique Model Decomposition (OM)

The technique of oblique incidence angle (Wang et al. 1995) is an extension of the original method by Farrell et al. (1992), in which the symmetry break between single scattered light near the entry point is measured relative to the diffuse part of the profile. The symmetry break allows an indirect measurement of the mean free path that eliminates the need for absolute intensity measurements. A major benefit to this is that it generally lowers the practical requirements of the vision system.

#### 3.3 Loglog Model Decomposition (LM)

Carstensen and Møller (2009) proposed the loglog model. It models the decay of the light intensity far away from the point of incidence. A double logarithmic transformed intensity profile ( $\log(\log(I+2))$ , where  $I$  is the pixel intensity) is extracted orthogonal to the scattering direction and through the point of incidence. A robust linear model is fitted to this profile, and the extracted feature is the slope parameter of this model. We have previously experienced very robust results with this decomposition method (unpublished).

### 3.4 Patch Average Decomposition (PA)

A point measurement from the diffuse reflectance images resembles the measurements made by fibre optic probes, where light is sent into the sample using one fibre and the diffuse reflection is collected by another fibre some distance from the incident light. The more times the light is scattered the lower the observed intensity will be. This is the main idea behind the work by Payne et al. (1993), which has proven itself useful in regard to determining the optimal cutting point during cheese making. As a light collecting fibre will often have a field of view, we select an image patch (50 by 50 pixels) orthogonal to the scattering direction and calculate a Gaussian weighted average of that patch. The patches will be extracted at different distances from the light incident point.

### 3.5 Intensity Spread Decomposition (IS)

A simple way to utilise a lot of the available image data is to consider histograms of the pixel intensities in the diffuse reflectance images. The histograms are created by masking out circular regions centred on the point of incidence. Typically histograms are quantified using first order statistics, however these are very sensitive to outliers. Since the distribution of the pixel intensities is heavy tailed, robust statistics should be considered. In the case of measuring the spread of the histogram we can use the median absolute deviation (MAD):

$$MAD = \text{median}(|X - \text{median}(X)|) \quad (1)$$

Which is the median of the absolute deviations from the median of the data ( $X$ ). The intensity spread will give an estimate of how the reflection intensity has developed after a given distance from the incident light point. As with the patch average decomposition, we consider different variations of the decomposition method, in this case by considering masks with different radii.

### 3.6 Feature Evaluation

The extracted features should be sensitive towards changes in scattering, such that small changes can be precisely assessed. They should also be robust with little variation within the same sample. We use the Rayleigh quotient, also known as the Fisher Criterion (Hastie et al. 2011) evaluate this property. It can be seen as an analogue to the signal-to-noise ratio (SNR), as it evaluates the between-class variance relative to the within-class variance. In the univariate case the Rayleigh quotient can be found as  $B/W$ , where  $B$  and  $W$  are the between- and within-class variances respectively. For best discrimination between different samples we want to have a large numerator and small denominator. In addition to the Rayleigh quotient we will also report the average leave-one-out classification results using linear support vector machine (SVM) classifiers (Chang and Lin 2011), to evaluate how well the different intralipid dilutions can be distinguished. The Rayleigh quotient and the SVM classification rates will be reported for the three different scattering regimes in the intralipid data set. Lastly we expect the 21 intralipid dilutions to have linearly increasing scattering properties. To verify this we report the correlation coefficient for the features in the entire scattering regime of the data set.

## 4 Results and Discussion

The results are summarized in Table 2. Overall the methods perform better in the low scattering regimes, and typically also at the higher wavelengths. These general observations hold true for the theoretical models (FM and OM). The two methods show similar trends both in terms of Rayleigh quotient and classification rates. They perform well in the low scattering regime, but degrade significantly when moving to the medium and high scattering regimes. The theoretical models behave well in terms of the expected linearity, and the low linearity for OM is simply because of large variance in the feature estimates. In general the theoretical models show more within class variation compared to the other methods. An example of the OM decomposition is shown in Fig. 2.

The LM decomposition performs well overall for the low and medium scattering regime in terms of classification. There is a significant drop in the Rayleigh quotient when going from the low to the medium scattering regime, hinting that while the method is robust, the sensitivity toward scattering changes is not as pronounced compared to PA or IS. However the linearity assumptions are maintained well, as can be seen in Fig. 2.

PA decomposition works very well for the low scattering regime and has the highest Rayleigh quotients in this regime. For the medium and highly scattering regimes there is a significant drop in performance, and there seems to be a serious problem in terms of linearity. This is especially prevalent when the patch is extracted far away from the point of incident. This is most likely because if a sample is highly scattering, the majority of

**Table 2** Evaluation of the different decomposition method at three different wavelengths. Each cell reports three numbers, one number for each of the three different scattering regimes (“low”/”medium”/”high”). Further a parameter,  $\beta$ , is provided for PA and IS. For PA it denotes how far away (in pixels) from the point of incident the patch is extracted, and for IS it denotes the radius (in pixels) of the applied mask.

### 500nm

Decomposition type	$\beta$	Rayleigh quotient	Classification rates [%]	Linearity
Farrell model (FM)	--	378.1 / 11.3 / 1.6	95.5 / 55.1 / 14.3	0.97
Oblique model (OM)	--	119.6 / 1.3 / 0.1	97.8 / 64.4 / 0	0.27
loglog model (LM)	--	1397.7 / 92.5 / 0.6	100 / 95.9 / 34.7	0.92
Patch average (PA)	100	254.1 / 183.6 / 29.3	100 / 91.8 / 59.2	0.86
	300	343.4 / 10.1 / 57.7	100 / 46.9 / 81.6	0.17
	500	254.2 / 44.1 / 15.7	79.6 / 65.3 / 77.6	0.39
Intensity Spread (IS)	100	152.0 / 54.8 / 10.3	100 / 77.6 / 42.9	0.97
	300	200.3 / 207.4 / 27.5	100 / 83.7 / 53.1	0.93
	500	252.1 / 235.2 / 34.4	100 / 91.8 / 73.5	0.88

### 700nm

Farrell model (FM)	--	84.1 / 20.6 / 1.5	98.0 / 57.1 / 20.4	0.93
Oblique model (OM)	--	73.4 / 6.2 / 0.7	90.5 / 62.5 / 20.5	0.64
loglog model (LM)	--	694.6 / 254.5 / 3.4	100 / 98.0 / 57.1	0.95
Patch average (PA)	100	1127.8 / 186.6 / 119.2	100 / 98.0 / 93.4	0.91
	300	3158.2 / 24.9 / 337.3	100 / 53.1 / 67.3	0.57
	500	3325.6 / 13.6 / 36.0	100 / 30.6 / 89.8	0.08
Intensity Spread (IS)	100	156.8 / 44.6 / 12.6	100 / 85.7 / 61.22	0.95
	300	722.3 / 354.1 / 94.5	100 / 100 / 87.8	0.94
	500	1263.4 / 511.3 / 212.4	100 / 100 / 89.8	0.92

### 900nm

Farrell model (FM)	--	31.7 / 12.3 / 1.4	69.4 / 69.4 / 28.6	0.98
Oblique model (OM)	--	65.4 / 25.9 / 3.9	100 / 72.5 / 43.3	0.97
loglog model (LM)	--	632.7 / 493.5 / 43.2	100 / 100 / 93.9	0.96
Patch average (PA)	100	556.7 / 354.8 / 45.7	100 / 95.9 / 89.8	0.99
	300	2004.5 / 209.1 / 2.9	100 / 85.7 / 14.3	0.89
	500	2646.0 / 9.2 / 33.4	100 / 44.9 / 44.9	0.64
Intensity Spread (IS)	100	134.52 / 31.3 / 9.2	100 / 79.6 / 42.9	0.99
	300	564.26 / 205.3 / 69.5	100 / 100 / 93.9	0.99
	500	1042.6 / 372.8 / 113.0	100 / 100 / 96.0	0.99

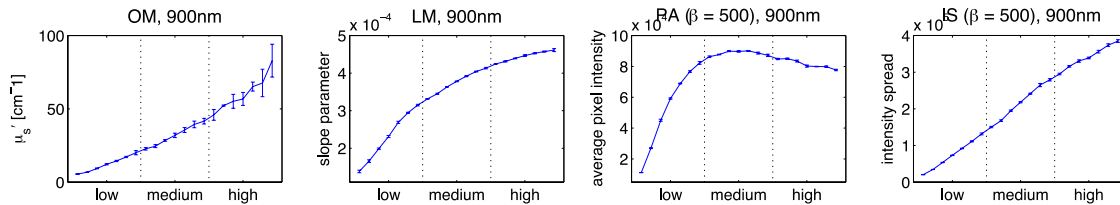


**Fig 2.** Examples of how different methods perform. The bars indicate the standard deviation for the feature estimates of the seven replicates for each dilution. The dotted lines indicate the different scattering regimes.

the diffusion dynamics happens close to the point of incidence, leaving very little variation between samples in the areas far from the point of incidence. Thus, feature estimates can reach a plateau when the scattering becomes sufficiently high. An example for PA with high discrimination (and reasonable linearity) for the low scattering regime, but bad linearity for entire regime can be found in Fig. 2.

The overall performance of the IS decomposition is good and it shows the best results throughout the entire scattering regime, while retaining the expected linear behaviour. This is especially true when looking at 900nm. The method performs best when the mask radius is large. Compared to PA the sensitivity is not as great in the low scattering regimes. The best performing IS decomposition example can be seen in Fig. 2.

From these results it is clear that no single decomposition method does not stand out as the better solution for the presented data set. It really depends on the considered scattering regime, the used wavelength, and the needed sensitivity and robustness. While the FM, OM, and LM decompositions are fairly fixed in the way they are extracted, the sampling schemes used for the PA and IS decompositions could have been done differently. Additionally two-dimensional spatial features have not been considered in this contribution. Furthermore the geometry of the vision system can also be changed, and especially increasing the amount of zoom used for the camera should significantly enhance the performance. More zoom would allow capturing

more details of the diffusion dynamics, which should increase the performance when the scattering becomes “too high”. This especially holds true for the theoretical models, as their underlying models depend on modelling these dynamics.

## 5 Conclusions

In this paper we have demonstrated some of the potential in using diffuse reflectance images. Both theoretical and data-driven decomposition methods were demonstrated and tested in practice. It was seen that by sacrificing some of the interpretability (and some practical advantages in the case of the oblique decomposition method) provided by the theoretical methods, significant increases in both robustness and sensitivity could be achieved. While some data driven methods successfully covered the entire considered scattering range, no single decomposition method performed best in all the considered data sets. This emphasises the advantage of considering diffuse reflectance images, when designing or optimizing instruments based on light reflectance methods.

## Acknowledgements

This work was (in part) financed by the Centre for Imaging Food Quality project, which is funded by the Danish Council for Strategic Research (contract no 09-067039) within the Programme Commission on Health, Food and welfare.

## References

- Alexander, M., Dalgleish, D.G., 2006, Dynamic light scattering techniques and their applications in food science, *Food Biophysics*, 1, 1, 2-13.
- Aguilera, J.M., Stanley, D.W., 1999, *Microstructural principles of food processing and engineering*, Springer.
- Aguilera, J.M., 2005, Why food structure?, *Journal of Food Engineering*, 67, 3-11.
- Bourne, M., 2002, *Food texture and viscosity: concept and measurement*, Academic Press.
- Carstensen, J.M., Møller, F., 2009, Online monitoring of food processes using subsurface laser scattering, *Advances in process analytics and control technologies APACT*, 5-7.
- Chandrasekhar, S., 1960, *Radiative Transfer*, Dover Publications.
- Chang, C.C., Lin, C.J., 2011, LIBSVM: A library for support vector machines, *ACM Transactions on Intelligent Systems and Technology*, 2, 3, 1-27.
- Farrell, T.J., Patterson, M.S., Wilson, B., 1992, A diffusion theory model of spatially resolved, steady-state diffuse reflectance for the noninvasive determination of tissue optical properties in vivo, *Med Phys*, 19, 4, 879-888.
- Frisvad, J.R., Christensen, N.J., Jensen, H.W., 2007, Computing the scattering properties of participating media using Lorenz-Mie theory, *ACM Transactions on Graphics (TOG)*, 26, 3, 60.
- Gowen, A.A., O'Donnell, C.P., Cullen, P.J., Downey, G., Frias, J.M., 2007, Hyperspectral imaging--an emerging process analytical tool for food quality and safety control, *Trends in Food Science & Technology*, 18, 12, 590-598.
- Hastie, T.J., Tibshirani, R., Friedman, J., 2011, *The elements of statistical learning: data mining, inference, and prediction*, Springer.
- MacGregor, J.F., Kourti, T., 1995, Statistical process control of multivariate processes, *Control Engineering Practice*, 3, 3, 403-414.
- Mann, S., Picard, R.W., 1994, Being undigital with digital cameras: Extending dynamic range by combining differently exposed pictures, *MIT Media Lab Perceptual*, 323.
- Michels, R., Foschum, F., Kienle, A., 2008, Optical properties of fat emulsions, *Opt. Express*, 16, 8, 5907-5925.
- Nielsen, O.H.A., Dahl, A.L., Larsen, R., Møller, F., Nielsen, F., Thomsen, C., Aanæs, H., Carstensen, J.M., 2011, Supercontinuum light sources for hyperspectral subsurface laser scattering, *Scandinavian Conference on Image Analysis*, 327-337.
- Payne, F.A., Hicks, C.L., Madangopal, S., Shearer, S.A., 1993, Fiber optic sensor predicting the cutting time of coagulating milk for cheese production, *Transaction of the ASAE*, 36.
- Qin, J., Lu, R., 2007, Measurement of the absorption and scattering properties of turbid liquid foods using hyperspectral imaging, *Applied spectroscopy*, 61, 4, 388-396.
- Sun, D.W., 2010, *Hyperspectral imaging for food quality analysis and control*, Academic Press.
- Wang, L., Jacques, S.L., 1995, Use of a laser beam with an oblique angle of incidence to measure the reduced scattering coefficient of a turbid medium, *Applied Optics*, 34, 13, 2362-2366.
- Weitz, D.A., Zhu, J.X., Durian, D.J., Gang, H., Pine, D.J., 1993, Diffusing-wave spectroscopy: the technique and some applications, *Physica Scripta*, 610.